IEEE Access
Multidisciplinary ⋮ Rapid Review ⋮ Open Access Journal

Received 6 February 2024, accepted 22 May 2024, date of publication 30 May 2024, date of current version 7 June 2024.

Digital Object Identifier 10.1109/ACCESS.2024.3407680

RESEARCH ARTICLE

6-DOF Vehicle Pose Estimation Considering Lidar Odometry Initial Condition

CHANUK YANG AND KUNSOO HUH, (Member, IEEE)
Department of Automotive Engineering, Hanyang University, Seoul 04763, South Korea

Corresponding author: Kunsoo Huh (khuh2@hanyang.ac.kr)

This work was supported by the Ministry of Trade, Industry, and Energy (MOTIE), South Korea, through the Technology Innovation Program (Development on Automated Driving with Perceptual Prediction Based on T-Car/Vehicle Parts to Intelligent Control/System Integration for Assessment) under Grant 20018101.

ABSTRACT Precise localization is essential for reliable autonomous driving. Traditionally, many systems have turned to lane level map matching techniques utilizing High Definition Maps (HD-Maps). However, it is necessary to have considerate efforts tied to the continuous availability and timeliness of these HD-Maps. Taking this into account, this paper explores an alternative approach, focusing on landmark-based odometry and a filtering-based technique. The proposed localization algorithm is integrated with the GPS and the odometry in a loosely coupled approach. Because it is important to obtain an initial pose in order to utilize the odometry, the initial odometry rotation is estimated from the filtering method, as an alternative to optimization methods, to improve the global consistency in localization. In addition, because specific landmark-based odometry, like lidar odometry, can become vulnerable in geometrically repetitive scenarios such as in tunnels, this study considers the change in vehicle speed and updates the landmark-based odometry, aiming to address the limitations. Through experimental tests in normal scenarios and challenging scenarios like tunnels, it is demonstrated that our method offers certain benefits over the existing techniques.

INDEX TERMS Localization, pose estimation, landmark-based odometry, Kalman filter, initialization.

I. INTRODUCTION

Precise vehicle localization plays a significant role in path planning and control for autonomous vehicles. Most self-driving cars utilize lane level map matching algorithms for accurate localization. Lane level map matching compares the vehicle's sensor data with a pre-existing High Definition Map (HD-Map) to determine its precise position. These algorithms allow for accurate estimation of the vehicle's location. However, creating detailed maps for all regions is a challenging task, and even if achievable, the dynamic nature of roads due to construction and other factors can make the maps less reliable.

Instead, landmark-based odometry is commonly implemented using SLAM (Simultaneous Localization and Mapping) algorithms, which simultaneously estimate the vehicle's pose and build the map. Recent state-of-the-art studies [1], [2], [3], [4], [5] show that filtering-based SLAM achieves high accuracy in real-time positioning.

The associate editor coordinating the review of this manuscript and approving it for publication was Shunfeng Cheng.

However, to effectively utilize odometry algorithms in vehicles, it is crucial to ensure global consistency and reliability with the actual vehicle sensors. Many research had focused on achieving global consistency using the GPS (Global Positioning System) [6], [7], [8]. The combination of the GPS with other methods can significantly affect the overall performance. For instance, loosely coupled approach integrates the positional data computed by the GPS receiver, whereas the tightly coupled approach utilizes raw satellite data, including wavelengths.

Regarding sensor integration for reliable odometry performance in vehicles, the most common strategy involves utilizing the vehicle's speed sensor [9], [10], [11], [12]. The loosely coupled approach uses vehicle speed or odometry pose, whereas the tightly coupled approach directly uses raw wheel encoder signals [9]. The choice of initial values can impact the performance in loosely coupled integration. While the tightly coupled approach can improve localization accuracy, it can be also sensitive to the vehicle's behavior. For instance, tire longitudinal slip on icy roads or side slip angle during high-speed turns may cause inconsistent localization performance.

In this paper, to overcome the limitations of the lane level map matching problem, a localization method is proposed by utilizing the landmark-based odometry. Instead of the resource-intensive optimization-based approach for odometry algorithms, a filtering-based odometry technique is adopted. In addition, a loosely coupled integration of odometry and the GPS is conducted based on vehicle speed. The translation and rotation reference frames are established based on the GPS, and the localization performance is enhanced by estimating the initial rotation. The proposed method is validated through experimental data of the autonomous driving. The main contribution of this study can be summarized as follows:

- Enhancement of the performance of landmark-based odometry by incorporating vehicle speed with a simpler approach.
- Demonstration of the performance difference depending on whether vehicle speed or wheel speed is used.
- Estimation of the initial rotation of odometry to achieve global consistency.
- Assessment of the feasibility by collecting and utilizing experimental autonomous vehicle data.

II. RELATED WORKS

Various filtering techniques, such as EKF (Extended Kalman Filter), UKF (Unscented Kalman Filter) and PF (Particle Filter), have been utilized for localization in a two-dimensional plane (3 DOF) [13], [14], [15], [16], and for 6 DOF localization based on the euler angle [17], [18], [19], [20]. However, localization based on euler angle can cause gimbal lock, and thus, more advanced filtering techniques are needed for rotation conversion.

Recently, the representative filtering methods used in localization are MSCKF (Multi State Constrained Kalman filter) and ESKF (Error State Kalman Filter) which can avoid the gimbal lock by using mathematical techniques, such as quaternion or lie group. The pioneering work introducing MSCKF was presented in [21], which utilized camera image features for updates. The evolved forms of MSCKF can be found in [22] and [23]. In [22], a scale factor to camera image data was added for estimation and was validated using simulations and real-world data. Sun et. al. [23] compared an optimization-based camera odometry with the MSCKF-based odometry, demonstrating accuracy and real-time performance advantages of the latter. MSCKF research mostly focused on camera-based implementations, and they showed superior real-time performance compared to optimization-based odometry.

ESKF (Error State Kalman Filter) has a similar structure to EKF, where the error state is estimated and added to the nominal state. A comprehensive explanation of ESKF can be found in [24], and most ESKF-based odometry studies adopted the algorithm described in [24]. Moreover, an iterative form of ESKF called IESKF (Iterative ESKF) was used in many lidar-based odometry approaches, achieving state-of-the-art performance [5]. Qin et al. [3] used filtering-based pose estimation and stored the map in a pose-graph format. In [4] and [5], the algorithm in [3] was modified to estimate the map in a tree structure, enhancing computation speed. Additionally, Bai et al. [25] demonstrated that the map structure can further improve computation speed. The IESKF-based lidar odometry not only improved the accuracy, but also was experimentally validated for real-time operation. They aimed to leverage the improved odometry performance in a loosely coupled manner. Similar approaches can be found in [26], where ESKF was used for global localization, and lidar odometry's position and rotation were incorporated.

Regarding the integration of odometry and the GPS, two approaches exist: one involves finding the initial pose globally and integrating it, while the other estimates poses relatively without an initial position. In [6], the GPS and odometry trajectories were matched using optimization techniques to achieve odometry consistency. Lee et al. [7] tightly coupled GPS's raw values with odometry for global consistency. These studies [6], [7] involved a trade-off between odometry's global consistency and GPS trajectory's length. Lynen et al. [8] combined odometry using relative poses without using the cumulative pose values. This approach allows updating global poses without knowing the initial values. However, this method requires careful consideration of time delays and synchronization between the GPS and odometry, especially in scenarios where the GPS reception is intermittent, like in tunnels.

Several studies have incorporated wheel speed into landmark-based odometry. In [9], wheel speed was combined with a 2D kinematic model to estimate the difference between IMU (Inertial Measurement Unit) pose and wheel pose in real-time. Filip et. al. [10] demonstrated the improved performance in feature-less tunnel scenarios when combining wheel encoders. In [11], errors occurring in wheel encoders and IMU were learned and estimated, resulting in enhanced localization performance. Dang et al. [12] incorporated wheel speed not only for position estimation, but also for wheel slip estimation.

On the other hand, in this study, by estimating the rotation matrix instead of the Euler angle, the 3D rotation of the vehicle is obtained, thereby preventing gimbal lock. The pose state is estimated using the ESKF algorithm. When the GPS data is available for reception, the GPS data is utilized to estimate the pose data alongside odometry data in a loosely coupled method. During this process, initial rotation of the odometry is estimated only upon receiving the GPS data. Conversely, in areas where the GPS reception is not available, only the odometry data is utilized. The estimated initial rotation remains fixed from when the GPS signal is not received. Additionally, lidar odometry, integrated with vehicle speed, is employed for application on highways.

III. PRELIMINARY

A. BOX PLUS, BOX MINUS OPERATOR IN MANIFOLD

Let $\mathcal{M}$ is a manifold of dimension. If the manifold is locally smooth, then bijective mapping can be performed between the

local neighborhood on $\mathcal{M}$ and the tangent space at that point. The operators that can perform bijective mapping are $\boxplus$ and $\boxminus$ operators, and the operation is expressed as follows [5]:

$$\begin{aligned}
&\boxplus : \mathcal{M} \times \mathbb{R}^n \to \mathcal{M};\\
&a \boxplus b = a + b; \quad \boldsymbol{R}_1 \boxplus r = \boldsymbol{R}_1 \exp{[r]_\times},\\
&\boxplus : \mathbb{R}^n \times \mathcal{M} \to \mathcal{M};\\
&b \boxplus a = b + a; \quad r \boxplus \boldsymbol{R}_1 = \exp{[r]_\times}\boldsymbol{R}_1,\\
&\boxminus : \mathcal{M} \times \mathcal{M} \to \mathbb{R}^n;\\
&a \boxminus b = a - b; \quad \boldsymbol{R}_2 \boxminus \boldsymbol{R}_1 = [\log(\boldsymbol{R}_2^T \boldsymbol{R}_1)]^\vee
\end{aligned}$$

where $\{a, b\} \in \mathbb{R}^n \subset \mathcal{M}, r \in \mathbb{R}^3$, and $\boldsymbol{R}_n \in SO(3) \subset \mathcal{M}$. $[\cdot]_\times$ and $[\cdot]^\vee$ are skew symmetric matrix operator of vectors and the inverse of skew symmetric matrix operator, respectively. For a compound manifold $\mathcal{M} = SO(3) \times \mathbb{R}^n$, the following relations are established:

$$\begin{bmatrix} R \\ a \end{bmatrix} \boxplus \begin{bmatrix} r \\ b \end{bmatrix} = \begin{bmatrix} R \boxplus r \\ a + b \end{bmatrix}; \quad \begin{bmatrix} R_2 \\ a \end{bmatrix} \boxminus \begin{bmatrix} R_1 \\ b \end{bmatrix} = \begin{bmatrix} R_2 \boxminus R_1 \\ a - b \end{bmatrix}$$

IV. MODIFICATION OF THE FAST-LIO ALGORITHM

The overall architecture of the algorithm proposed in this paper is illustrated in Figure 1. While the conventional odometry (Fast-LIO) leveraged the synergy between Lidar and IMU, our study incorporates vehicle speed into the residual computation segment to facilitate state updates. Next, in the ESKF-based pose estimation phase, the output pose value from the odometry is utilized for correction and the GPS pose is employed for estimating the states defined in the ESKF localization.

A. SUMMARY OF THE FAST LIO ALGORITHM

The Fast LIO [5] is a tightly coupled, direct feature based Lidar-Inertial Odometry algorithm. Unlike other optimization-based algorithms, Fast LIO is formulated as a filtering-based approach. The Fast LIO formulated the equations mathematically to reduce the computational load associated with the number of features. This formulation can handle a large number of features efficiently. Moreover, the algorithm improved the accuracy by utilizing direct features instead of line or plane features, enabling it to handle numerous features.

Furthermore, while other optimization-based approaches utilize graph-based maps, incremental kd-tree data structure was adopted to construct the map, contributing to faster computations [4], [5].

B. VEHICLE SPEED AIDED FAST-LIO ALGORITHM

The weakness of the Fast-LIO is its difficulty in handling repetitive features. For instance, when passing through tunnels, Lidar's nature of measuring distances can lead to the repeated appearance of static features. If the vehicle's speed remains constant, the IMU value will also be constant, resulting in serious errors and problems with SLAM algorithm performance. To address this issue, this study introduces the addition of a vehicle speed error to handle the repetitive features.

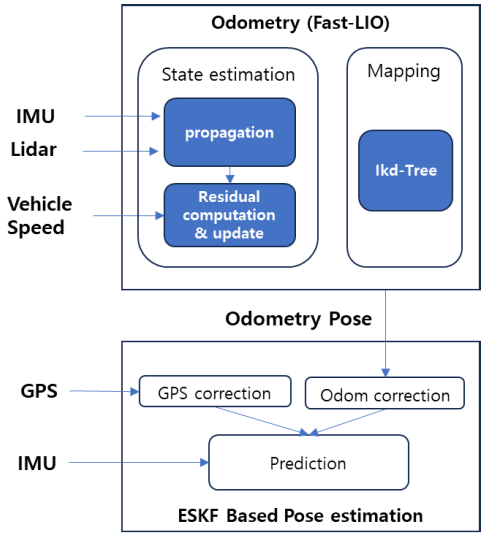

FIGURE 1. Architecture of the proposed algorithm.

Because the vehicle speed value is available by the vehicle CAN signal, it can be directly utilized to model the data. The residuals between vehicle speed from the CAN signal and the estimated vehicle speed are defined as follows:

$$z_s^\kappa = ||v_I^\kappa||_2 - s_{veh} \tag{1}$$

where v_I^κ is the estimated velocity of the IMU in the odometry algorithm with the iterated update (κ). s_{veh} is the speed of the vehicle from the CAN signal. $||v_I^\kappa||_2$ is the norm of the velocity from the IMU and the residual in equation (1) can be extracted invariantly regardless of the vehicle speed direction. Considering the noise of vehicle speed, the measurement model, h_s, can be expressed as follows:

$$h_s(\mathbf{x}_k, n_s) = ||v_I||_2 - (s_{veh} - n_s) \tag{2}$$

where n_s accounts for the noise in the vehicle speed measurement and $\mathbf{x}_k$ is the IMU state defined in the odometry algorithm. Approximating the above equation by its first order differential leads to

$$\begin{aligned}
h_s(\mathbf{x}_k, n_s) &\simeq h_s(\bar{\mathbf{x}}_k^\kappa, 0) + H_s^\kappa \tilde{\mathbf{x}}_k^\kappa + n_s\\
&= z_s^\kappa + H_s^\kappa \tilde{\mathbf{x}}_k^\kappa + n_s
\end{aligned} \tag{3}$$

where $\bar{\mathbf{x}}_k^\kappa$ and $\tilde{\mathbf{x}}_k^\kappa$ are the predicted nominal state and state error of the IMU in the odometry algorithm with the iterated update (κ), respectively. Also, H_s^κ represents the Jacobian matrix of $h_s(\mathbf{x}_k, 0)$.

In the original Fast-LIO, feature updates are performed using the Iterated Error State Kalman Filter (IESKF), and the MAP (Maximum A-Posteriori) was defined as follows [5]

$$\min_{\tilde{\mathbf{x}}_k^\kappa}(||\mathbf{x}_k \boxminus \bar{\mathbf{x}}_k||^2_{\bar{P}_k^{-1}} + \Sigma_{j=1}^m ||\mathbf{z}_j^\kappa + H_j^\kappa \tilde{\mathbf{x}}_k^\kappa||^2_{\sigma_j^{-1}}) \tag{4}$$

where $||\mathbf{x}||^2_M = \mathbf{x}^T M \mathbf{x}$. $\bar{P}_k$, σ_j, and m are the predicted state covariance of IMU, standard deviation of noise in the

single lidar point, and the number of lidar points, respectively. The first term in equation (4) is the quadratic cost of prior distribution of $\mathbf{x}_k$, and the second term is the quadratic cost of lidar point residual. To incorporate the vehicle speed, the above equation is modified in this study.

$$\min_{\widetilde{\mathbf{x}}_k^\kappa}(||\mathbf{x}_k \boxminus \bar{\mathbf{x}}_k||^2_{\bar{P}_k^{-1}} + \Sigma_{j=1}^{M}||\mathbf{z}_j^\kappa + H_j^\kappa \widetilde{\mathbf{x}}_k^\kappa||^2_{\sigma_j^{-1}} + ||z_s^\kappa + H_s^\kappa \widetilde{\mathbf{x}}_k^\kappa||^2_{\sigma_s^{-1}}) \quad (5)$$

where σ_s is standard deviation of noise in the vehicle speed. The first and second terms are the same as the original Fast-LIO algorithm, but the third term is newly added including the vehicle speed residual. To apply this equation, the IESKF method is utilized, and Jacobian in equation (5) includes the concatenation of H_j and H_s from the original IESKF equations.

V. LOCALIZATION ALGORITHM FOR GLOBAL CONSISTENCY

A. IMU KINEMATIC MODEL [24]

The Error State Kalman Filter (ESKF) is utilized as the backend algorithm for the pose estimation. The main objective of the ESKF is to minimize the error term in the state. Aiming for the states associated with 3D rotation to converge to zero makes it particularly advantageous over the conventional Kalman Filter (KF) or Extended Kalman Filter (EKF). Consequently, this method separates the error state from the nominal state and applies them accordingly. The discrete Inertial Measurement Unit (IMU) model for the nominal state can be expressed based on accelerometer data, a_m, and gyroscope data, w_m, [24].

$$\begin{aligned}
\bar{R}_{t+1} &= R_t \exp([(w_m - b_{w,t})\Delta t]_\times) \\
\bar{p}_{t+1} &= p_t + v_t \Delta t + 0.5(R_t(a_m - b_{a,t}))\Delta t^2 \\
\bar{v}_{t+1} &= v_t + (R_t(a_m - b_{a,t}))\Delta t \\
\bar{b}_{a,t+1} &= b_{a,t} \\
\bar{b}_{w,t+1} &= b_{w,t}
\end{aligned} \quad (6)$$

where R_t is the rotation matrix, p_t is the position, v_t is the velocity. $b_{a,t}, b_{w,t}$ and Δt are the biases for the accelerometer, gyroscope at timestep t and difference of timestep, respectively. The terms with $\bar{\cdot}$ (bar) means the predicted variables from the nominal IMU model. The discrete error state model is shown below from the continuous-time model [24]:

$$\begin{aligned}
\delta\theta_{t+1} &= (\exp[(w_m - b_{w,t})\Delta t]_\times)^T \delta\theta_t - \delta b_{w,t}\Delta t + n_\theta \\
\delta p_{t+1} &= \delta p_t + \delta v_t \Delta t \\
\delta v_{t+1} &= \delta v_t + (-R_t[a_m - b_{a,t}]_\times \delta\theta - R_t \delta b_{a,t})\Delta t + n_v \\
\delta b_{a,t+1} &= n_{b,a} \\
\delta b_{w,t+1} &= n_{b,w}
\end{aligned} \quad (7)$$

where $n_\theta, n_v, n_{b,a}$, and $n_{b,w}$ are noise terms for rotation, velocity, accelerometer bias, and gyroscope bias, respectively. The terms with δ indicate the error values for the corresponding variables, and θ_t is the rotation vector of R_t.

B. ESKF LOCALIZATION

The ESKF equations consist of the prediction and correction steps as the conventional Kalman filter. The prediction step is expressed as follows [24]:

$$\bar{x}_{t+1} = f_x(\widehat{x}_t, u_m). \quad (8)$$

$$\bar{P}_{t+1} = F_x \widehat{P}_t F_x^T + F_i Q_i F_i^T \quad (9)$$

where $\bar{x}_t$ is the predicted state by the nominal prediction model, $f_x(\widehat{x}_t, u_m)$. $\widehat{P}_t$ is the covariance of error state and F_x is the linear error state model. $\widehat{x}_t$ and u_m are the estimated state vector at time step t and input data, respectively. F_i and Q_i are noise matrix and covariance matrix of the noise impulses, respectively. It is essential to note that the predicted error state is always converging to zero and needs not to be predicted by the model. However, the covariance of error state is important and needs to be predicted by the linear error state model. The correction step of the ESKF can be expressed as follows:

$$\widetilde{x}_{t+1} = K(z - h(\bar{x}_{t+1})) \quad (10)$$

$$K = \bar{P}_{t+1} H^T (H \bar{P}_{t+1} H^T + V)^{-1} \quad (11)$$

$$\widehat{P}_{k+1} = (I - KH)\bar{P}_{t+1}(I - KH)^T + KVK^T. \quad (12)$$

$$\widehat{x}_{k+1} = \bar{x}_{t+1} \boxplus \widetilde{x}_{t+1}. \quad (13)$$

where z, $h(\bar{x}_t)$ and V are the measurement vector, the measurement model, and the noise matrix of the measurement vector, respectively. K is the Kalman gain and H is the Jacobian matrix of the error state from the measurement model. $\widetilde{x}_{t+1}$ is the corrected error of the estimated state. This formulation is almost same as the conventional Kalman filter except equation (13), which indicates that the estimated state is obtained by combining the error state with the predicted state. The operator, $\boxplus$, is explained in section III.

C. ESTIMATION OF ODOMETRY INITIAL ROTATION

For actual implementation of odometry to maintain global consistency, the initial rotation and translation must be aligned. Even if it is assumed that odometry outputs an accurate position, a difference in values can occur depending on the initial position. If the translation position changes slightly, the difference from the actual value might not have a large impact as it is only as much as the difference in translation. However, if the initial rotation deviates by even 0.1 degrees, it can cause a significant impact as the distance increases. In this study, the initial rotation of odometry is estimated to reduce such impacts. A model for the initial rotation is first defined as follows with the subscript i representing the initial state:

$$\dot{R}_i = I, \delta\dot{\theta}_i = 0, \quad (14)$$

or, in discrete form,

$$\bar{R}_{i,t+1} = R_{i,t}, \delta\theta_{i,t+1} = \delta\theta_{i,t} \quad (15)$$

The model implies that there should be no change in the initial rotation model and the error state should approach zero.

Then, the states are combined with the initial rotation model and IMU model.

$$\widehat{x}_t = \begin{bmatrix} p_t \\ v_t \\ R_t \\ b_{a,t} \\ b_{w,t} \\ R_{i,t} \end{bmatrix}, \bar{x}_t = \begin{bmatrix} \bar{p}_t \\ \bar{v}_t \\ \bar{R}_t \\ \bar{b}_{a,t} \\ \bar{b}_{w,t} \\ \bar{R}_{i,t} \end{bmatrix}, \widetilde{x}_t = \begin{bmatrix} \delta p_t \\ \delta v_t \\ \delta\theta_t \\ \delta b_{a,t} \\ \delta b_{w,t} \\ \delta\theta_{i,t} \end{bmatrix} \triangleq \begin{bmatrix} \widetilde{x}_{t,l} \\ \widetilde{x}_{t,g} \end{bmatrix} \quad (16)$$

In equation (16), $\bar{x}_t$ and $\widehat{x}_t$ belong to the Manifold ($\mathcal{M}$), and $\widetilde{x}_t$ belongs to the vector space ($\mathbb{R}^{18}$). Furthermore, $\widetilde{x}_t$ is divided into $\widetilde{x}_{t,l}$ and $\widetilde{x}_{t,g}$, which are terms related to the local coordinate ($\delta p_t, \delta v_t, \delta\theta_t, \delta b_{a,t}, \delta b_{w,t}$), and global coordinate ($\delta\theta_{i,t}$), respectively. The local coordinate is displayed based on the location of the IMU. If the state is established as in equation (16), formulas (8)-(12) can be still applied. In the prediction step (equations (8) and (9)), F_x, F_i and Q_i can be expressed by combining equation (7) with the initial rotation.

$$F_x = \begin{bmatrix} I & I\Delta t & 0 & 0 & 0 & 0 \\ 0 & I & A & -R_t\Delta t & 0 & 0 \\ 0 & 0 & B & 0 & -I\Delta t & 0 \\ 0 & 0 & 0 & I & 0 & 0 \\ 0 & 0 & 0 & 0 & I & 0 \\ 0 & 0 & 0 & 0 & 0 & I \end{bmatrix},$$

$$F_i = \begin{bmatrix} 0 & 0 & 0 & 0 \\ I & 0 & 0 & 0 \\ 0 & I & 0 & 0 \\ 0 & 0 & I & 0 \\ 0 & 0 & 0 & I \\ 0 & 0 & 0 & 0 \end{bmatrix},$$

$$Q_i = \begin{bmatrix} n_v I & 0 & 0 & 0 \\ 0 & n_\theta I & 0 & 0 \\ 0 & 0 & n_{b,a} I & 0 \\ 0 & 0 & 0 & n_{b,w} I \end{bmatrix}$$

$$\text{where} \quad A = -R_t[a_m - b_{a,t}]_\times \Delta t,$$
$$B = (\exp[(w_m - b_{w,t})\Delta t]_\times)^T \quad (17)$$

Meanwhile, in the correction step, a loosely coupled fusion is conducted using GPS pose and odometry pose data. To fuse each data, the coordinates of each sensor and the world coordinates must be accurately defined and represented. The relationships of each coordinate are illustrated in Figure 2. The notation ${}_Ap^B$ and ${}_AR^B$ represent the relative position and rotation of B frame in A frame, respectively. For example, ${}_Ip^G$ and ${}_IR^G$ denote the relative position and rotation of the GPS frame in the IMU frame. In this figure, the entities represented in dark blue, ${}_Wp^I$, ${}_WR^I$, and ${}_OR^W$ correspond to p_t, R_t, and $R_{t,i}$ in equation (16), respectively. Also, it is assumed that the relative position between odometry frame and world frame is zero. In this study, ${}_Op^I$ and ${}_OR^I$ are utilized as the odometry measurement data, and are defined as p_z^I and R_z^I, respectively. Also, ${}_Wp^G$ and ${}_WR^G$ are utilized as the GPS measurement data, and are defined as p_z^G and R_z^G, respectively. The GPS measurement model from the World frame to the GPS frame,

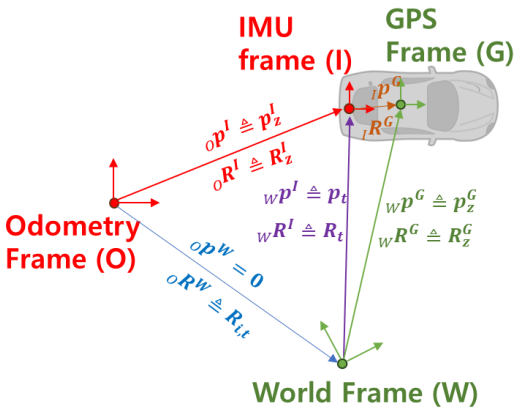

FIGURE 2. Transformation relations with GPS frame, Odometry frame, IMU frame, and world frame.

$h_G(x_t)$, can be established as follows.

$$h_G(x_t) = \begin{bmatrix} R_t\,{}_Ip^G + p_t \\ [\log(R_t\,{}_IR^G)]^\vee \end{bmatrix} \quad (18)$$

where ${}_Ip^G$ and ${}_IR^G$ are the calibration data of position and rotation from IMU to GPS coordinate systems. The residual vector of the GPS measurement can be expressed as follow:

$$r_G = z_G - h_G(x_t) = \begin{bmatrix} p_z^G - (R_t\,{}_Ip^G + p_t) \\ \theta_z^G - [\log(R_t\,{}_IR^G)]^\vee \end{bmatrix} \quad (19)$$

where $z_G = [p_z^G, \theta_z^G]^T$. θ_z^G is the rotation vector of R_z^G. It is necessary to obtain the Jacobian of the measurement model to utilize in the correction step from equations (11) to (12). The Jacobian of the GPS measurement model can be expressed as follows:

$$H_G = \frac{\partial h_G(x)}{\partial \delta x}\Big|_{x=\bar{x}_t} = \begin{bmatrix} I_3 & \mathbf{0}_{3,3} & -R_t[{}_Ip^G]_\times & \mathbf{0}_{3,3} & \mathbf{0}_{3,3} & \mathbf{0}_{3,3} \\ \mathbf{0}_{3,3} & \mathbf{0}_{3,3} & C & \mathbf{0}_{3,3} & \mathbf{0}_{3,3} & \mathbf{0}_{3,3} \end{bmatrix}$$

$$\text{where} \quad C = \begin{bmatrix} \mathbf{0}_{3,1} & I_3 \end{bmatrix} [q_t]_L [{}_Iq^G]_R \begin{bmatrix} \mathbf{0}_{1,3} \\ I_3 \end{bmatrix} \quad (20)$$

where q_t and ${}_Iq^G$ are quaternion vectors of R_t and ${}_IR^G$, respectively. Also, $[\cdot]_L$ and $[\cdot]_R$ are the left- and right-quaternion-product matrix operators, respectively [24]. The Kalman gain in equation (11) is obtained by replacing H with H_G, and the correction step from the GPS measurement is performed as in equations (10)-(13). The odometry measurement model from the odometry frame to the IMU frame, $h_o(x_t)$, can be represented as position and orientation.

$$h_o(x_t) = \begin{bmatrix} h_p(x_t) \\ h_\theta(x_t) \end{bmatrix} = \begin{bmatrix} R_{i,t}p_t \\ [\log(R_{i,t}R_t)]^\vee \end{bmatrix} \quad (21)$$

where the $h_p(x_t)$ and $h_\theta(x_t)$ are position measurement model and rotation measurement model from the odometry frame to the IMU frame. Then, the residual vector of the odometry measurement, r_o, can be defined as follows:

$$r_o = z_o - h_o(x_t) = \begin{bmatrix} p_z^I - R_{i,t}p_t \\ \theta_z^I - [\log(R_{i,t}R_t)]^\vee \end{bmatrix} \quad (22)$$

where $z_o = [p_z^I, \theta_z^I]^T$. θ_z^I is the rotation vector of R_z^I. The Jacobian of the odometry measurement model can be expressed considering the initial rotation:

$$H_o = \frac{\partial h_o(x)}{\partial \delta x}\Big|_{x=\bar{x}_t} = \begin{bmatrix} \frac{\partial h_p(x)}{\partial \delta p_t} & \mathbf{0}_{3,3} & \mathbf{0}_{3,3} & \mathbf{0}_{3,3} & \mathbf{0}_{3,3} & \frac{\partial h_p(x)}{\partial \delta \theta_{i,t}} \\ \mathbf{0}_{3,3} & \mathbf{0}_{3,3} & \frac{\partial h_\theta(x)}{\partial \delta \theta_t} & \mathbf{0}_{3,3} & \mathbf{0}_{3,3} & \frac{\partial h_\theta(x)}{\partial \delta \theta_{i,t}} \end{bmatrix} \quad (23)$$

The 10 blocks on the left inside of H_o are Jacobian terms that are often used in a loosely coupled manner. Besides, the 2 vertical blocks on the right side are terms added to estimate the initial rotation. Through this method, the estimated initial rotation allows correction to continue as the odometry value is received. In the same manner as in GPS measurement correction, the Kalman gain in equation (11) is obtained by replacing H with H_o, and the correction step from odometry measurement is performed as in equations (10)-(13). Each Jacobian term inside H_o can be expressed as follows:

$$\frac{\partial h_p(x)}{\partial \delta p_t} = R_{i,t} \quad (24)$$

$$\frac{\partial h_p(x)}{\partial \delta \theta_{i,t}} = -[R_{i,t} p_t]_\times \quad (25)$$

$$\frac{\partial h_\theta(x)}{\partial \delta \theta_t} = \begin{bmatrix} \mathbf{0}_{3,1} & I_3 \end{bmatrix} [q_{i,t} \otimes q_t]_L \begin{bmatrix} \mathbf{0}_{1,3} \\ I_3 \end{bmatrix} \quad (26)$$

$$\frac{\partial h_\theta(x)}{\partial \delta \theta_{i,t}} = \begin{bmatrix} \mathbf{0}_{3,1} & I_3 \end{bmatrix} [q_{i,t} \otimes q_t]_R \begin{bmatrix} \mathbf{0}_{1,3} \\ I_3 \end{bmatrix} \quad (27)$$

where $q_{i,t}$ is quaternion vector of $R_{i,t}$, and $\otimes$ is quaternion product operator [24]. If equation (13) is directly applied, it may not be possible to estimate the odometry rotation initialization. This is because the remaining states excluding the odometry initial rotation must correct the error state on the IMU frame, but the odometry initial rotation must correct the error state on the world frame. For this reason, after equation (13) is modified and applied, the estimated state is decribed as follows:

$$\widehat{x}_{t+1} = \begin{bmatrix} \mathbf{0}_{15} \\ \widetilde{x}_{t,g} \end{bmatrix} \boxplus \bar{x}_{t+1} \boxplus \begin{bmatrix} \widetilde{x}_{t,l} \\ \mathbf{0}_3 \end{bmatrix} \quad (28)$$

The states in the local frame are added to the back of equation (13), while the odometry initial rotation in the global frame is added to the front.

VI. EXPERIMENTAL RESULTS

A. EXPERIMENTAL SETUP

In this study, experimental data is utilized to validate the proposed algorithm. The test vehicle is depicted in Figure 3, and its setup incorporates the GPS and the IMU units. These two units are synergistically integrated to generate a GPS-IMU SPAN (Synchronous Position, Attitude and Navigation) solution [27]. To enhance the positional accuracy of the GPS, Network RTK is employed. For the LiDAR setup, a 32-channel lidar is mounted at the center, complemented by 16-channel LiDAR modules on both sides. The chassis CAN data was also collected to measure wheel speed and vehicle speed signals.

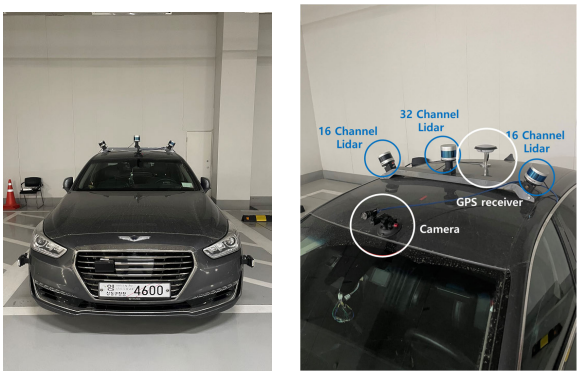

FIGURE 3. Sensor setup in test vehicle.

B. QUALITATIVE ODOMETRY PERFORMANCE EVALUATION FROM DRIVING MANEUVER

In this experiment, tests are executed on both low-friction straight roads and curved roads. The primary objective is to evaluate the difference between the conventional and modified Fast-LIO algorithms when longitudinal slip occurs in the roads. Straight road tests are carried out in regions with sparse features extracted in lidar odometry, with braking applied on the low-friction surface. The performance among the conventional Fast-LIO, GPS-IMU and the modified algorithms are presented. In Figure 4, red line represents the conventional Fast LIO, green line denotes the GPS-IMU, blue line indicates the wheel-speed-based modification of the Fast-LIO, and yellow line reflects the vehicle-speed-based modification of the Fast-LIO. The conventional Fast-LIO encounters errors in localization performance, mainly due to the challenge of accurately estimating the position through lidar odometry, especially when the sparse features are detected. In the case of the modified Fast-LIO utilizing the wheel speed, a notable error in the displacement was observed during braking on low-friction surfaces, exceeding that of the GPS-IMU measurements. This results underscore potential inadequacies in the algorithm when it relies on the wheel speed signal. On the contrary, integrating the vehicle speed with the Fast-LIO, rather than the wheel speed, produced results that closely matched with the GPS-IMU solution. This result demonstrate a significant improvement in the performance of the Fast-LIO due to its dependence on Lidar, IMU, and particularly on vehicle speed signals.

Figure 5 presents the experimental results conducted on curved, low-friction roadways involving consistent cornering and braking maneuvers. In this case, the conventional Fast-LIO achieved satisfactory results, similar to those of the vehicle-speed-based modification of the Fast-LIO. However, the wheel-speed-based Fast-LIO exhibited large errors in position estimation. Despite feature detection from the lidar, speed errors caused by wheel slip can affect the Fast-LIO algorithm to estimate the position data inaccurately.

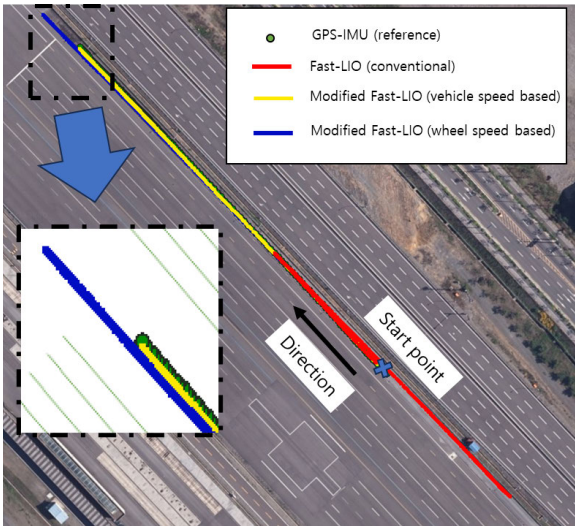

FIGURE 4. Odometry performance evaluation in straight open road.

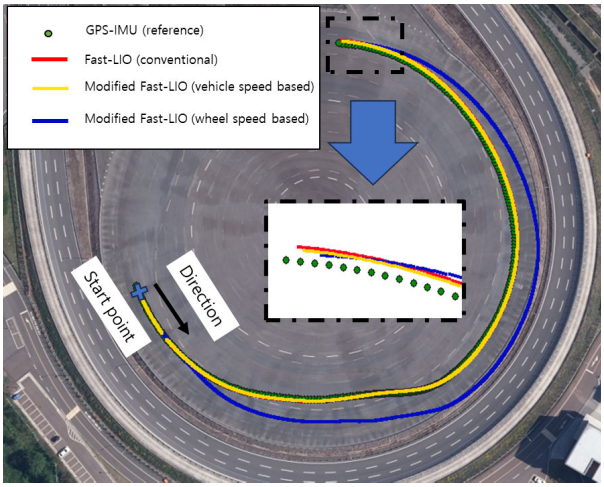

FIGURE 5. Odometry performance evaluation in circular open road.

C. RESULTS OF ODOMETRY INITIAL ROTATION

This section focuses on validating the functionality of initial rotation estimation in the proposed algorithm. Scenario setup involves the test vehicle driving on a motorway, performing straight-line, turning, and lane-changing maneuvers. During these tests, the GPS-IMU signals and Fast-LIO pose values are provided correctly. Figure 6 illustrates the odometry initial rotation estimation results when the initialized value is sourced from GPS-IMU SPAN solution data. Contrary to the case (dotted line) without estimation of the initial rotation, the roll, pitch, and yaw errors converge almost to zero without significant fluctuations, indicating accurate estimation of odometry initial rotation.

In the same experimental context, Figure 7 illustrates the results when the yaw value of the odometry initial rotation is initialized with 75 degrees biased. In this case, because the GPS-IMU SPAN solution provides INS high variance status flag about the rotation angle, GPS rotation angle values are not used in the estimation. Therefore, this result also explores the accuracy of the estimation by relying solely on

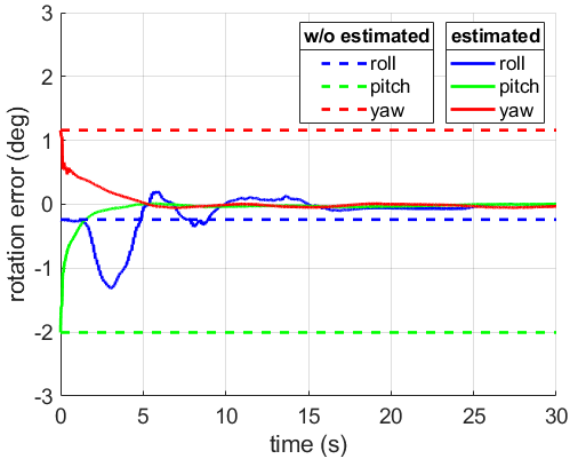

FIGURE 6. Odometry initial rotation estimation results initialized from GPS rotation.

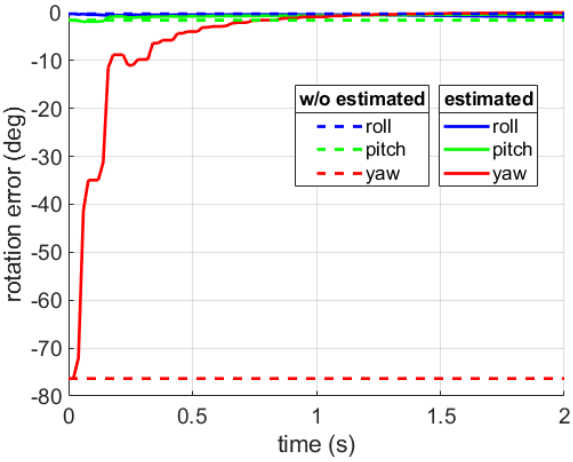

FIGURE 7. Odometry initial rotation estimation results initialized from biased GPS rotation.

GPS position data. Despite the bias in the initial odometry rotation values and the exclusion of GPS rotation signals from the measurement data, the results of yaw error is observed to converge around zero. This convergence suggests that the proposed method for estimation of odometry initial rotation is effective, utilizing filtering techniques based on GPS position measurement.

D. LOCALIZATION PERFORMANCE EVALUATION IN HIGHWAY SCENARIO INCLUDING TUNNEL

Additional experiments are performed on highways with tunnels to evaluate the efficacy of the proposed algorithm. The test route spans approximately 10.9 kilometers and passes through the tunnel in several sections. As a result, the GPS-RTK signal is less reliable and its positioning accuracy becomes challenging. Therefore, using GPS-IMU signals as a reference is impractical. Instead, to obtain the ground truth in this experiment, an optimization process is utilized that integrates wheel speed, GPS, IMU, and preexisting maps. The optimization process is developed from the GTSAM Library [28]; when GPS signals are available, both the GPS pose prior factor and the IMU preintegration factor are employed.

TABLE 1. Localization performance in highway scenario including tunnel.

Case	Lateral Error(m)		Longitudinal Error(m)		Roll Error(deg)		Pitch Error(deg)		Yaw Error(deg)	
	mean	1σ	mean	1σ	mean	1σ	mean	1σ	mean	1σ
GPS-IMU	13.3	20.3	7.08	9.50	**1.21**	0.94	1.24	**0.17**	**0.58**	**0.25**
J.Sola [24]	18.3	19.1	8.34	9.71	1.37	1.99	1.65	3.11	0.85	0.98
Proposed (with initial est)	**2.78**	**3.64**	**5.60**	**6.69**	1.28	**0.86**	**0.83**	0.58	0.67	0.41

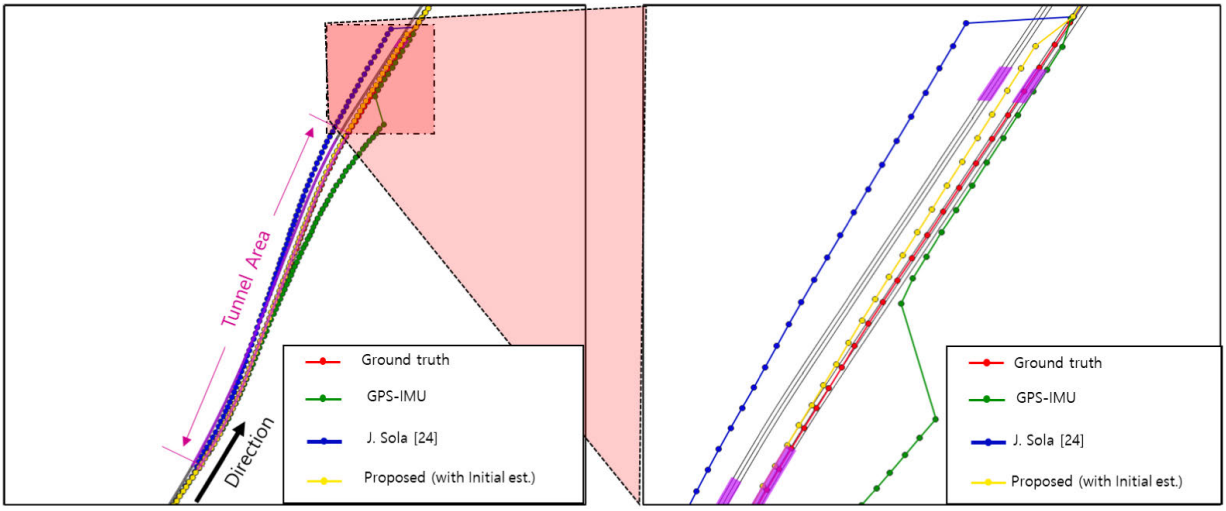

FIGURE 8. Performance results in curved tunnel scenario, including reference position data.

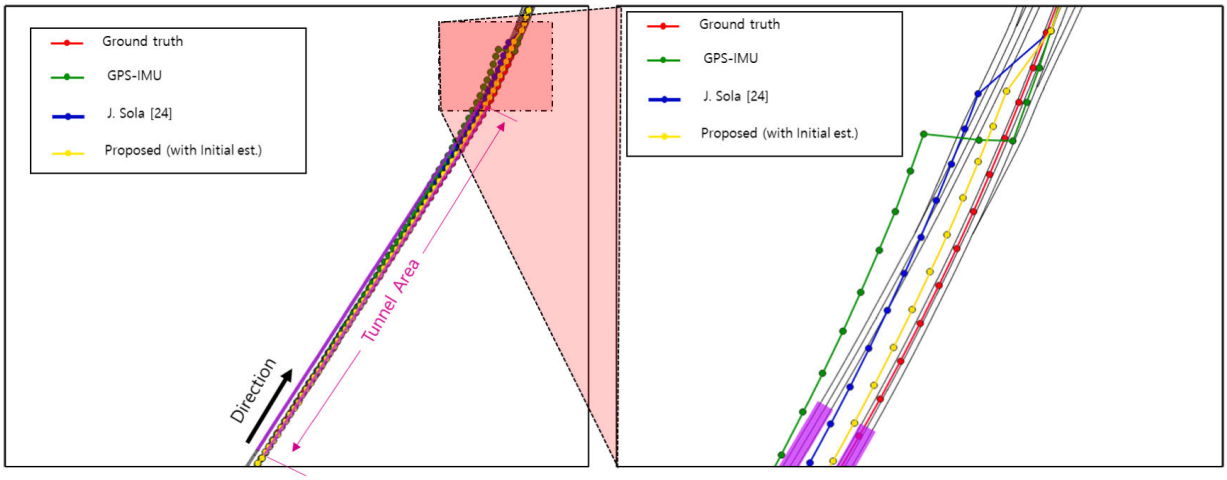

FIGURE 9. Performance results in straight tunnel scenario, including reference position data.

On the contrary, in areas with poor GPS signal, wheel odometry-based factors and positional prior factors based on map waypoints are applied.

To evaluate algorithm performance in this experiment, deviations are represented in terms of longitudinal and lateral errors, as well as roll, pitch, and yaw errors. Additionally, to verify the performance inside tunnels, localization results with semantic map and reference path are presented. Three algorithms are compared; GPS-IMU, Sola [24], and the proposed algorithm. The algorithm based on Sola [24] utilizes the measurements from the GPS and the pose data from odometry algorithm. The algorithm strictly fixes the initial position and rotation of the GPS while running the odometry for position estimation. On the contrary, the proposed algorithm with initial rotation estimation incorporates the proposed initial rotation estimation to operate the odometry for position estimation. Pose data comparisons are conducted at one-second intervals.

Table 1 presents the performance results for GPS-IMU, Sola [24], and proposed algorithm. Both longitudinal and lateral deviations indicate that the proposed algorithm demonstrates the best performance among comparison methods. This highlights the importance of integrating odometry with initial rotation estimation. Meanwhile, the performances in terms of roll, pitch, and yaw are comparable between the GPS-IMU and the proposed algorithm.

Figures 8 and 9 highlight the results observed when exiting tunnels. Figure 8 presents results when driving out of curved tunnels, while Figure 9 depicts outcomes when exiting straight tunnel roads. In both scenarios, the incorporation

of odometry improves the performance compared to relying solely on GPS-IMU. In particular, the longitudinal and lateral deviation demonstrates the enhanced accuracy in comparison to GPS-IMU. Besides, the effect of the initial rotation estimation is evident both inside and after exiting the tunnel area. This suggests that our algorithm provides crucial insights for addressing the challenges associated with localization deviation inside and after tunnels.

VII. CONCLUSION

For autonomous vehicle localization, this study suggests alternatives beyond the conventional lane-level map matching techniques that rely on High Definition Maps (HD-Maps). Recognizing the challenges and unreliability associated with HD-Maps, this research introduces a modified approach using landmark-based odometry. A modification on the Fast-LIO algorithms with utilizing vehicle speed, as opposed to wheel speed, provides better results. This method can solve the problem of repetitive geometry, such as in tunnels, by adjusting the landmark-based odometry relative to vehicle speed. Besides, in tunnel regions on highways, the integration of the GPS with odometry, particularly with including initial rotation estimation, proves to enhance global consistency.

REFERENCES

[1] P. Geneva, K. Eckenhoff, W. Lee, Y. Yang, and G. Huang, "OpenVINS: A research platform for visual-inertial estimation," in *Proc. IEEE Int. Conf. Robot. Autom. (ICRA)*, May 2020, pp. 4666–4672.

[2] W. Lee, P. Geneva, C. Chen, and G. Huang, "MINS: Efficient and robust multisensor-aided inertial navigation system," 2023, *arXiv:2309.15390*.

[3] C. Qin, H. Ye, C. E. Pranata, J. Han, S. Zhang, and M. Liu, "LINS: A LiDAR-inertial state estimator for robust and efficient navigation," in *Proc. IEEE Int. Conf. Robot. Autom. (ICRA)*, May 2020, pp. 8899–8906.

[4] W. Xu and F. Zhang, "FAST-LIO: A fast, robust LiDAR-inertial odometry package by tightly-coupled iterated Kalman filter," *IEEE Robot. Autom. Lett.*, vol. 6, no. 2, pp. 3317–3324, Apr. 2021.

[5] W. Xu, Y. Cai, D. He, J. Lin, and F. Zhang, "FAST-LIO$_2$: Fast direct LiDAR-inertial odometry," *IEEE Trans. Robot.*, vol. 38, no. 4, pp. 2053–2073, Aug. 2022.

[6] W. Lee, K. Eckenhoff, P. Geneva, and G. Huang, "Intermittent GPS-aided VIO: Online initialization and calibration," in *Proc. IEEE Int. Conf. Robot. Autom. (ICRA)*, May 2020, pp. 5724–5731.

[7] W. Lee, P. Geneva, Y. Yang, and G. Huang, "Tightly-coupled GNSS-aided visual-inertial localization," in *Proc. Int. Conf. Robot. Autom. (ICRA)*, May 2022, pp. 9484–9491.

[8] S. Lynen, M. W. Achtelik, S. Weiss, M. Chli, and R. Siegwart, "A robust and modular multi-sensor fusion approach applied to MAV navigation," in *Proc. IEEE/RSJ Int. Conf. Intell. Robots Syst.*, Nov. 2013, pp. 3923–3929.

[9] W. Lee, K. Eckenhoff, Y. Yang, P. Geneva, and G. Huang, "Visual-inertial-wheel odometry with online calibration," in *Proc. IEEE/RSJ Int. Conf. Intell. Robots Syst. (IROS)*, Oct. 2020, pp. 4559–4566.

[10] I. Filip, J. Pyo, M. Lee, and H. Joe, "LiDAR slam with a wheel encoder in a featureless tunnel environment," *Electronics*, vol. 12, no. 4, p. 1002, 2023.

[11] M. Brossard and S. Bonnabel, "Learning wheel odometry and IMU errors for localization," in *Proc. Int. Conf. Robot. Autom. (ICRA)*, May 2019, pp. 291–297.

[12] Z. Dang, T. Wang, and F. Pang, "Tightly-coupled data fusion of VINS and odometer based on wheel slip estimation," in *Proc. IEEE Int. Conf. Robot. Biomimetics (ROBIO)*, Dec. 2018, pp. 1613–1619.

[13] F. Dellaert, D. Fox, W. Burgard, and S. Thrun, "Monte Carlo localization for mobile robots," in *Proc. IEEE Int. Conf. Robot. Autom.*, vol. 2, May 1999, pp. 1322–1328.

[14] L. D'Alfonso, W. Lucia, P. Muraca, and P. Pugliese, "Mobile robot localization via EKF and UKF: A comparison based on real data," *Robot. Auto. Syst.*, vol. 74, pp. 122–127, Dec. 2015.

[15] X. Xia, N. P. Bhatt, A. Khajepour, and E. Hashemi, "Integrated inertial-LiDAR-based map matching localization for varying environments," *IEEE Trans. Intell. Vehicles*, vol. 8, no. 10, pp. 4307–4318, Oct. 2023.

[16] L. Teslić, I. Škrjanc, and G. Klančar, "EKF-based localization of a wheeled mobile robot in structured environments," *J. Intell. Robotic Syst.*, vol. 62, pp. 187–203, May 2011.

[17] B. Allotta, L. Chisci, R. Costanzi, F. Fanelli, C. Fantacci, E. Meli, A. Ridolfi, A. Caiti, F. Di Corato, and D. Fenucci, "A comparison between EKF-based and UKF-based navigation algorithms for AUVs localization," in *Proc. OCEANS Genova*, May 2015, pp. 1–5.

[18] G. P. C. Júnior, A. M. Rezende, V. R. Miranda, R. Fernandes, H. Azpúrua, A. A. Neto, G. Pessin, and G. M. Freitas, "EKF-loam: An adaptive fusion of LiDAR slam with wheel odometry and inertial data for confined spaces with few geometric features," *IEEE Trans. Autom. Sci. Eng.*, vol. 19, no. 3, pp. 1458–1471, Apr. 2004.

[19] N. Akai, T. Hirayama, and H. Murase, "3D Monte Carlo localization with efficient distance field representation for automated driving in dynamic environments," in *Proc. IEEE Intell. Vehicles Symp. (IV)*, Oct. 2020, pp. 1859–1866.

[20] N. Akai, "Reliable Monte Carlo localization for mobile robots," *J. Field Robot.*, vol. 40, no. 3, pp. 595–613, 2023.

[21] A. I. Mourikis and S. I. Roumeliotis, "A multi-state constraint Kalman filter for vision-aided inertial navigation," in *Proc. IEEE Int. Conf. Robot. Autom.*, Apr. 2007, pp. 3565–3572.

[22] S. Weiss and R. Siegwart, "Real-time metric state estimation for modular vision-inertial systems," in *Proc. IEEE Int. Conf. Robot. Autom.*, May 2011, pp. 4531–4537.

[23] K. Sun, K. Mohta, B. Pfrommer, M. Watterson, S. Liu, Y. Mulgaonkar, C. J. Taylor, and V. Kumar, "Robust stereo visual inertial odometry for fast autonomous flight," *IEEE Robot. Autom. Lett.*, vol. 3, no. 2, pp. 965–972, Apr. 2018.

[24] J. Solà, "Quaternion kinematics for the error-state Kalman filter," 2017, *arXiv:1711.02508*.

[25] C. Bai, T. Xiao, Y. Chen, H. Wang, F. Zhang, and X. Gao, "Faster-LIO: Lightweight tightly coupled LiDAR-inertial odometry using parallel sparse incremental voxels," *IEEE Robot. Autom. Lett.*, vol. 7, no. 2, pp. 4861–4868, Apr. 2022.

[26] H. Li, L. Pan, and J. Zhao, "LiDAR-aided visual-inertial localization with semantic maps," in *Proc. IEEE/RSJ Int. Conf. Intell. Robots Syst. (IROS)*, Oct. 2022, pp. 910–916.

[27] S. Kennedy, J. Hamilton, and H. Martell, "Architecture and system performance of SPAN-NovAtel's GPS/INS solution," in *Proc. IEEE/ION PLANS*, Apr. 2006, pp. 266–274.

[28] F. Dellaert, "Factor graphs and GTSAM: A hands-on introduction," Center Robot. Intell. Mach., Georgia Inst. Technol., Tech. Rep. GT-RIM-CP&R-2012-002, 2012, p. 4, vol. 2.

CHANUK YANG received the B.S. degree in mechanical system and design engineering from Hongik University, Seoul, Republic of Korea, in 2016. He is currently pursuing the Ph.D. degree with the Department of Automotive Engineering. His research interests include vehicle localization, which is precise pose estimation from any other sensers and map, and state estimation, and which is monitoring the vehicle state from partially observed data.

KUNSOO HUH (Member, IEEE) received the Ph.D. degree from the University of Michigan, Ann Arbor, MI, USA, in 1992. He is currently a Professor with the Department of Automotive Engineering, Hanyang University, Seoul, South Korea. His research interests include machine monitoring and control, with emphasis on their applications to vehicular systems, sensor-based active safety systems, V2X-based safety systems, autonomous vehicle control, and AI applications in autonomous vehicle.